Proceedings of the XVth Bi-Annual Symposium on Measuring Techniques in Transonic and Supersonic Flows in Cascades and Turbomachines, 21-22 September, Florence, Italy

A Study of the Frequency Response of a Micro Machined Shear-Stress Sensor Based on Thin Film Anemometry.

S. Gjerstad S, Y. Fu, H.P. Hodson , W.N. Dawes and D.F. Moore
Cambridge University, Department of Engineering, Trumpington of Street, Cambridge, CB2 1PZ, UK

ABSTRACT

This paper describes an analysis of the performance of micro machined thin-film thermal anemometers for the measurement of surface shear-stress in air flows. Particular emphasis is placed upon improving the frequency response of the sensor and its thermal footprint. This is achieved by a miniaturisation of the sensor and by thermally isolating the sensor from the substrate upon which it is mounted.

The performance of several sensors has been modelled using a range of numerical methods. All of the sensors are capable of being manufactured using MEMS-based production techniques. The sensor with the highest frequency response consists of a heated metallic film that is supported on a suspended beam. The beam is flush mounted with the surface. The beam is thermally insulated from the supporting material by an air filled cavity. This reduces the conductive heat loss to the supporting material and minimises the *effective* dimensions of the sensor. It was found that the frequency response was improved when the bridge was made from silicon rather than an insulating material. Flow visualisation experiments have been carried out to demonstrate that the sensor causes no disturbance to the flow.

INTRODUCTION

Wall shear stress measurements can reveal important information about flow separation and transition in turbomachinery and external flow situations. In order to capture the best possible details of the flow, the wall shear stress sensor needs to have a small spatial resolution and a high frequency response in order to have a time constant of at least the same magnitude as the flow features and the eddies that are to be captured. For example, a low-pressure turbine aerofoil might operate at a Reynolds number of 200,000. Transition of the suction side boundary layer (or separation if transition does not occur) may begin at a Reynolds number based on the momentum thickness of approximately 200. If the chord is 40 mm, this gives a momentum thickness of approximately 0.04 mm at the point of transition. The largest eddies are characterised by a dimension which is approximately 10 times this value and they convect at approximately 70 percent of the freestream velocity which will approach the sonic value. Thus, a frequency response of the order of 0.5 MHz is required simply to see the largest eddies.

Direct and indirect methods exist for measuring wall shear stress in a fluid flow. A direct measurement of shear stress is obtained by mechanically measuring the viscous force experienced by a small floating element mounted at the surface. The drag force represents the area integration of the shear force (Liu et al). The spatial resolution of the floating element can be improved by using micro machining manufacturing techniques. An increase in frequency response can also result. the highest frequency response is limited by the lowest natural frequency f_n for the floating element and is given by (Goldstein)

$$f_n = \frac{1}{2p}\sqrt{\frac{k}{m}} \qquad (1)$$

where f_n is the natural frequency of the floating element, m is the mass of the element and k is the spring constant. Unfortunately, a high frequency response results in a low sensitivity of the wall shear stress sensor due to the high stiffness required and these will not be considered further.

When using indirect methods of measuring the wall shear stress, the shear stress is related to measurements of, say, the difference between the wall static pressure and the pressure in a Preston or Stanton tube (Goldstein) or the heat transfer from an electrically heated thin-film element mounted on the surface. Only the heated film is considered here because other methods have a low temporal resolution and because they cause disturbances to the flow (Liu et al).

To relate the surface shear stress to the heat transfer from a heated element at the surface Bellhouse and Schultz (1966) solved the thermal-energy integral equation for steady laminar flow

$$ak^2 t_W \left(\frac{\Delta T}{q''}\right)^3 - \frac{1}{2} b \frac{\P p}{\P x} k^3 \left(\frac{\Delta T}{q''}\right)^4 = -\frac{m^2 L}{rks} \qquad (2)$$

where a and b are constants dependent on the velocity profile of the boundary layer, p, m, r, k and s are pressure, viscosity, density, conductivity and Prandtl number of the fluid, and ΔT is the

temperature difference between the hot film and free stream temperature. The dimension L is the *effective* streamwise length of the heated element. This is not the physical length but the streamwise length over which the heat transfer occurs. It is larger than the physical dimensions of the hot film because lateral conduction occurs within the substrate on which the sensor is mounted. The rate of heat transfer per unit area from the heated film to the flow is q''. By rearranging equation (2) and by assuming that there is a negligible pressure gradient the surface shear stress is shown to be

$$t_W^{1/3} = \left(\frac{m^2}{r\,sa L^2} \right)^{1/3} \left(\frac{q'' L}{k \Delta T_0} \right) \tag{3}$$

from which it can be seen that

$$q'' \propto t_W^{1/3} \tag{4}$$

so that the heat transfer from a heated element at the surface can be used to determine the surface shear stress.

Freymuth (1977) presented an analysis of the frequency response of the constant temperature hot wire anemometer. The same analysis can be used here. In the case of the "maximally flat" response curve, the cut-off frequency of the anemometer is given by

$$f_{cut} = \frac{1}{2p} \left(\frac{W_n^2 G}{M} \right)^{1/3} \tag{5}$$

where W_n^2 is the natural frequency of the amplifier, which is assumed to behave as a second order system in time (see Figure 1 for the circuit analysed by Freymuth), G is the amplifier gain and the time constant M of the sensor is given by

$$M = \frac{(1+n)^2}{2n} \frac{R_{hot}}{R_{hot} - R_{cold}} \frac{m_{sensor} c_p}{h A_{sensor}} \tag{6}$$

where n is the ratio of the sensor resistance R_{hot} to R_1 when the bridge is in balance, and m_{sensor}, c_p and A_{sensor} represent the mass, the specific heat capacity and the surface area of the sensor respectively.

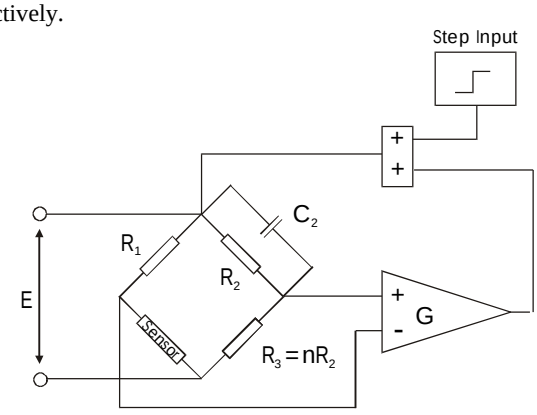

Figure 1 Constant temperature anemometer control circuit of Freymuth (1977). Step input only used for transient analysis. The capacitor C_2 is not used here

In the context of a surface mounted thin-film, equation (5) may be rewritten as

$$f_{cut} \propto \frac{hWL}{WLtrc_P} = \frac{h}{trc_P} \tag{7}$$

where L, W and t are the streamwise length, width and the thickness of the film respectively. Equation (3) can also be used to give

$$h \propto \frac{1}{L^{1/3}} \tag{8}$$

where h is the heat transfer coefficient. Combining equation (8) and equation (7) and assuming that the linear dimensions remain in proportion to each other reveals that the frequency response for a hot film scales with

$$f_{cut} \propto \frac{1}{L^{4/3}} \tag{9}$$

which is also true for a sensor operating in the constant current mode.

Currently available commercial sensors have a streamwise length that is typically 0.1 mm. They also have a frequency response that is of the order of 25 kHz. To obtain a frequency response of the order of 1 MHz, equation (9) indicates that the streamwise length must be reduced to approximately 5 μm. Micromachining technology can produce geometries in the micron range and in large quantities at a relatively low cost.

A NEW SENSOR GEOMETRY

Traditional hot film sensors are electrically heated thin films mounted on an insulating layer that is directly mounted on the surface of interest. This produces a continuous surface that causes no disturbance to the flow.

There are three main issues when designing a new shear stress sensor based on the micromachining technique. Firstly, the use of micromachining imposes geometrical constraints due to the techniques used to produce MEMS. Secondly, it is generally desirable to thermally insulate the heated element from the substrate. In doing so, the thermal footprint of the sensor is reduced which increases the spatial resolution. Furthermore, the effective thermal capacity is reduced and this serves to increase the frequency response. Thirdly, the sensor should not disturb the downstream flow so that a streamwise array of sensors may be used.

Figure 2 Schematic cross-section of the bridge (green) with the hot film (red) and the air gap around the bridge. *Not to scale*

At the outset of this project, it was decided that the heated film must be physically separated from the surrounding surface. This was required in order to maximise the frequency response and to minimise the thermal footprint. This can be achieved by placing a small air gap around the sensor. An example of this is shown in Figure 2 which reveals a heated film located on the top of a "bridge" with an air gap around the bridge. An isometric view of

the shear stress sensor can be seen in Figure 3. Red indicates electrical material, green is the bridge and blue is the silicon surface layer.

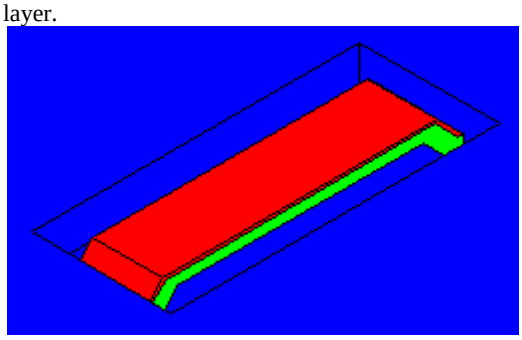

Figure 3 Isometric view of the hot film (red) mounted on the bridge (green) located in the cavity. *Not to scale*

Several different designs of hot film sensors have been manufactured using MEMS technology. For example, Liu et al placed the heated films on a thin silicon nitride membrane which was positioned above and evacuated cavity to insulate the sensor from the substrate. The membrane is relatively simple to make using micromachining technology and the sensor causes no disturbance to the flow because of the continuous surface. The sensor of Figure 2 was also placed on a membrane to produce a hybrid design as shown in Figure 4. These types of sensor and the conventional type which is placed directly on the substrate are both compared to that shown in Figure 2 and Figure 3.

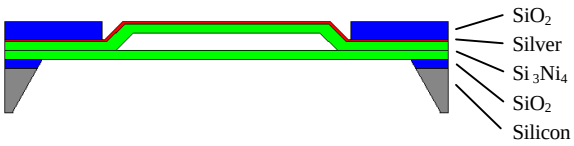

Figure 4 Cross section of sensor mounted on a bridge mounted on a membrane

The sensor presented in this paper has been designed for use in a typical turbomachinery flow environment. It has been assumed that of the coefficient of the skin friction is equal to 0.005, that the chord of a typical blade is 40 mm, that the Reynolds number ranges from 100,000 to 1,000,000. Assuming that the properties of air are those at standard atmospheric conditions, it is found that the streamwise length of 5 μm is equal to between 1.25 and 6.25 wall units ($1.25<L^+<6.25$; L is the streamwise length), depending on the Reynolds number. The critical wall roughness for turbulent flow is of the order of 5 wall units.

STEADY STATE ANALYSIS

In this section, the sensitivity and the thermal footprint are evaluated with the help of a finite element model of four types of sensors. These are the sensor mounted directly on a solid substrate; the sensor mounted on a thin membrane; the sensor mounted on a bridge; and the sensor mounted on a bridge on a membrane.

All of the heat transfer calculations were performed by the FEM program ABAQUS. A numerical procedure was developed so that the sensor could be operated in the constant temperature mode under steady state or transient conditions. This could be done because of the ability of ABAQUS to calculate a time dependent coupled thermal-electrical problem. Figure 1 shows the Wheatstone bridge with the feedback loop. The FEM program provides the resistance of the sensor at a given time. The resistance is typically of the order of a few tens of Ohms. The Wheatstone bridge is modelled in FORTRAN and the entire procedure including the ABAQUS calculation is automated using a script.

The sensor has two planes of symmetry. Therefore, the computational domain was restricted to one-quarter of the physical space. Initially, a computational domain of 5x5x5 mm was used to model the sensor on the solid substrate, on the membrane and on the bridge. The domain was later reduced to 200x200x200 μm in order to improve the spatial resolution of the computational mesh close to the sensor. This did not have an adverse effect on the far field calculation. To create a membrane, the rear surface of the silicon layer would the etched away. On the upper surface, the flow was assumed to be at 300 K and the heat transfer coefficient was specified. At the outer extremities of the computational domain, the temperature was set equal to 300 K.

The surface heat transfer coefficient of the sensor was determined using equation (3). The constant a is equal to 0.2226 in this case. The other parameters are given above. Thus, the convective heat transfer coefficient from a sensor is found to be

$$2000 \le h \le 10000 \qquad (10)$$

where the limits are determined by the range of Reynolds numbers. These are very high compared to typical values of the heat transfer coefficient in forced convection. Furthermore, it was assumed that there was no heat transfer from the surface of the substrate to the flow and that the only heat transfer by convection from the sensor occurred through the surface that was directly exposed to the mainstream flow. The justification for this is presented later in this paper.

The hot film used for the heat transfer calculations measured 100x5x0.1 μm. It was made of silver. The connecting wires were not modelled because of the added complexity. The absence of these wires will reduce the conduction from the hot film to the substrate. In turn, this will reduce the power input and, in the case of the transient calculations, increase of the frequency response. In the case of the sensor mounted on of the bridge, the air gap beneath the 1 μm thick bridge was also 1 μm. The upstream and downstream gaps measured 2 μm.

The coupled calculation procedure is operated in a time-marching mode until convergence to steady state is obtained. The calculation begins with the hot film at ambient conditions. A small current is passed through the sensor by applying a small voltage to the top of the bridge. For a small time increment, ABAQUS is used to calculate the resulting unsteady temperature field in the sensor and the substrate, and the new resistance of the sensor at the end of the time step. Unless convergence has been achieved, the differential amplifier increases the bridge voltage (which is not allowed to exceed a preset value) so that the current passing through the sensor is increased. The final temperature and resistance of the sensor are determined by the values of the other resistances in the Wheatstone bridge.

Figure 5 shows the thermal footprint for three different configurations. These are: the shear stress sensor mounted directly on solid silicon; the sensor mounted on a silicon nitride membrane 1.5 μm thick, as the used by Liu et al; and the sensor mounted on a silicon nitride bridge. The fourth arrangement, where the bridge is mounted on a membrane, is not shown because the results are identical to the third case. The maximum temperature of the sensor in each of the results shown in Figure 5 is the same. The required

power input to reach the maximum temperature of 475 K is shown in the individual captions. The power decreases from 335 mW when the sensor is mounted on a solid substrate to 2.37 mW when the sensor is mounted on the bridge.

Figure 5 shows that a large thermal footprint exists for both the sensor mounted on silicon and the sensor mounted on silicon nitride membrane. Indeed, the thermal footprint was larger in the latter case because there is no conduction from the membrane to the underlying substrate in the surface-normal direction. Because the thermal footprint is so large, the sensor will have a relatively poor yaw sensitivity and a relatively poor spatial resolution. In the case of the sensor mounted on a bridge, the thermal footprint is essentially that of the sensor so that the spatial resolution and the yaw sensitivity are significantly improved.

No thermal footprint exists for the case when the sensor is mounted on a bridge. This is because of the thermal insulation of the heated sensor from the surface. It should be recalled that the gap is assumed to be a perfect insulator. Filling the gap with still air did not significantly alter the results of the calculations. The CFD calculations described below reveal that the velocities within the gap are extremely low so that a still air approximation is reasonable.

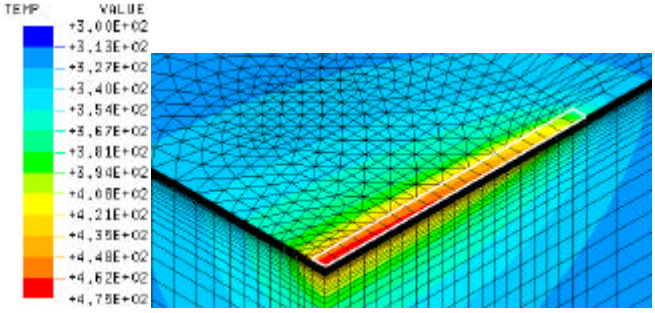

Sensor on solid. Power =335 mW

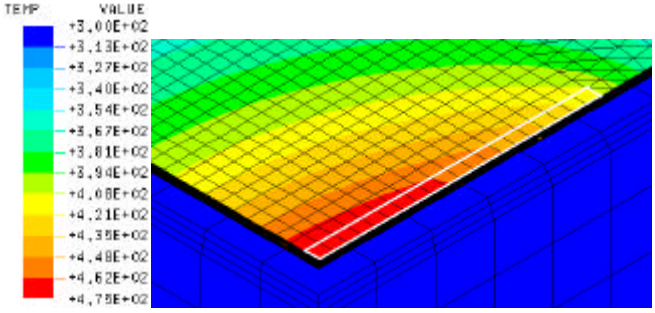

Sensor on membrane. Power =4.38 mW

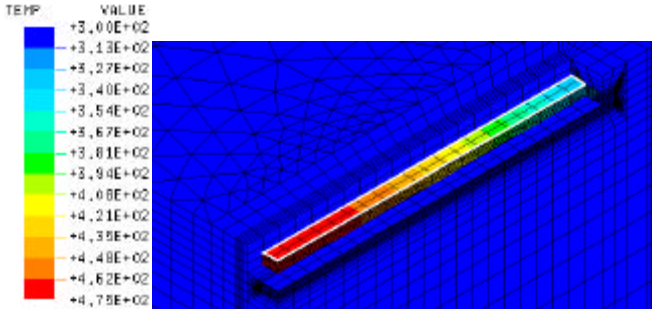

Sensor on bridge. Power = 2.37 mW

Figure 5 Temperature distribution in Kelvin of three sensor configurations. *(White line outlines the hot film)*

The sensitivity of the shear stress sensor can be represented as the ratio between heat convected to the fluid and the heat conducted into the substrate. The greater this ratio is the higher the sensitivity of the sensor. Heat conducted to the substrate is represented by term B in equation (11).

$$i^2R = \Delta T(A \cdot t_w^{1/3} + B) \qquad (11)$$

where i^2R is the ohmic heating of the hot film, ΔT is the temperature difference between the hot film and free stream. The constants A and B represent the fluid properties and that of the properties of the substrate respectively.

The smaller the value of the constant B in equation (11), the smaller the heat loss to the substrate. This in turn increases the sensitivity of the sensor. Figure 6 shows how the maximum temperature of the sensor varies with the power input to the sensor. In addition to the results for the three configurations shown in Figure 5, the result for a fourth configurations is shown. This configuration corresponds to the hybrid of a hot film mounted on a bridge which in turn is mounted on a membrane, both made from silicon nitride. It was found that the sensitivity of the sensor was increased with physical separation of the shear stress sensor from the substrate and by using insulating materials for the sensor support, such as silicon nitride and silicon oxide.

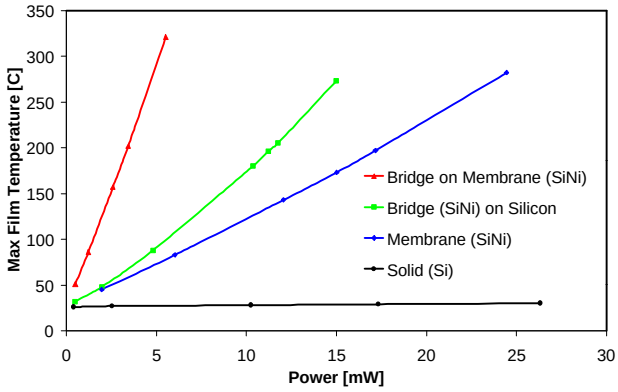

Figure 6 Maximum sensor temperature obtained for the four different sensor configurations

Figure 6 shows that the use of the silicon nitride membrane, as proposed by Liu et al, represents a significant improvement over the solid configuration. However it must be remembered that in this case, there is a substantial thermal footprint, as shown by Figure 5. Mounting of the hot film on a bridge which in turn is mounted on a silicon substrate improves the situation further.. Therefore, Figure 6 shows that an increase in the thermal resistance which represents the conduction to the substrate has the benefit of reducing the power supplied to the hot film. This in turn increases the sensitivity of the sensor because a larger proportion of the heat loss from the sensor is due to convection to the fluid and not conduction to the substrate.

TRANSIENT RESPONSE ANALYSIS

The coupled Wheatstone bridge model (coded in FORTRAN) and the unsteady ABAQUS calculation were used to assess the transient response of each of the four configurations described above. Once the bridge had reached equilibrium after being switched on, a step input signal was added to the top of the bridge so that the bridge was no longer in equilibrium. In effect, this is one half of the "square wave test" that is traditionally used to optimise the higher frequency performance of a constant

temperature anemometer. By repeating the FORTRAN and ABAQUS calculations until equilibrium is again achieved, it is possible to estimate the frequency response of the given configuration. Given that a number of assumptions have been made in order to perform these analyses, it should be noted that these results are indicative of the performance that could be obtained rather than true predictions of the performance.

In addition to the hot film configurations described above, a traditional hot wire with no supports, a length of 1 mm and a diameter of 5 μm was analysed to provide a reference and validation case. The results of this simulation are presented in Figure 7 in the form of the bridge voltage against time. The calculation shows that the frequency response is of the order of 100 kHz, which is similar to the measured frequency response of a an actual hot wire with the same geometry. In this case, the heat transfer coefficient was provided by King's Law. It is noted that the final voltage is not the same as the initial voltage. This is due to the bias created by the additional voltage supplied by the step input. The magnitude of the difference is related to the gain of the operational amplifier

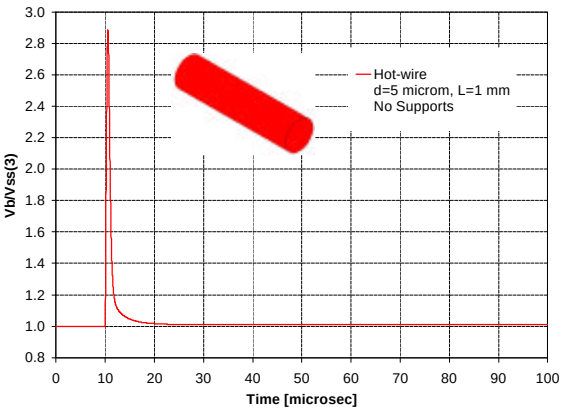

Figure 7 Frequency response of a 1 mm long and 5 μm diameter hot wire

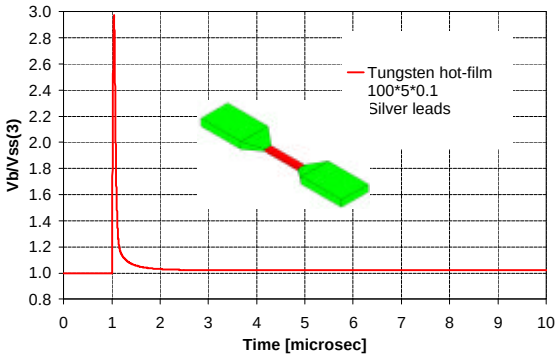

Figure 8 Frequency response of the heated element with no support

If only the heated element with size 100x5x0.1 μm made from tungsten and silver leads are simulated then the frequency response is estimated to be about 1 MHz. The time sensor voltage history can be seen in Figure 8. Of course, the sensor cannot be used without a bridge to support the thin film. As a result, the thermal mass of the system will increase and the frequency response of the sensor will decrease. It was found that the frequency response of the system is dependent on the material used for the bridge. Figure 9 shows the frequency response of two different bridge support materials. A bridge made from silicon nitride (thermal conductivity = 0.19 W/cm.K) resulted in a frequency response of 170 kHz compared to a frequency response of 500 kHz when using a silicon bridge (thermal conductivity = 1.57 W/cm.K). This means that a higher frequency response is obtained by using a bridge of higher thermal conductivity. In this case a silicon bridge will have a frequency response three times higher than that of a silicon nitride bridge.

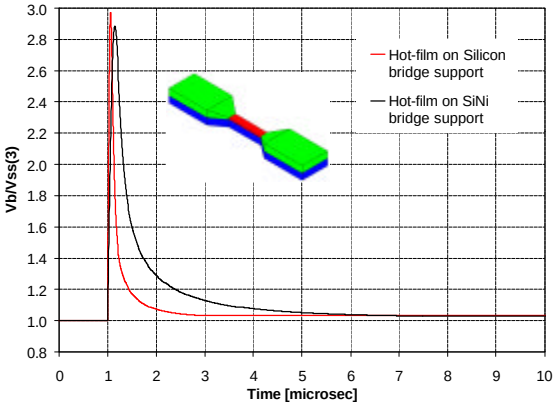

Figure 9 Frequency response of the heated element with 1.5 μm bridge of a silicon or silicon nitride

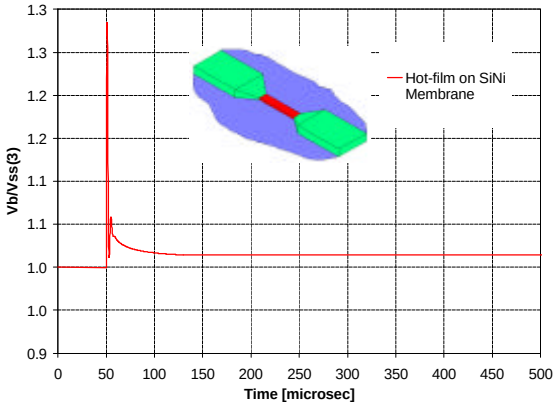

Figure 10 Frequency response of the heated element with 1.5 μm silicon nitride membrane

Figure 10 presents the voltage history for the case when the sensor is mounted on a 1.5 μm thick silicon nitride membrane. It should be noted that the abscissa has a very different scale to that of the previous figures. The reason for the oscillation of the sensor voltage immediately after the applied step is the long time step needed for this particular analysis. The long time step causes the Wheatstone bridge to overcompensate for the change in bridge voltage. Ideally the time step should have been shorter to avoid this but insufficient the CPU time was available. Whatever the case, the solution after a short period of time is independent of the time step used. In this case, the frequency response of the sensor is only 15 kHz. Liu et al reported that the time constant obtained for this type of sensor was equivalent to a frequency response of 14 kHz

CFD CALCULATION OF THE FLOW AROUND THE SENSOR

Predictions of the flow over and around the shear stress sensor were obtained using the unstructured Navier-Stokes code (NEWT) of Dawes. Because the aspect ratio of the sensor is of the order of 20:1, three-dimensional aspects were not considered. These are only important about the ends of the sensor where it is connected to the substrate. A flow visualisation experiment using a water flume confirmed that the end effects are minor.

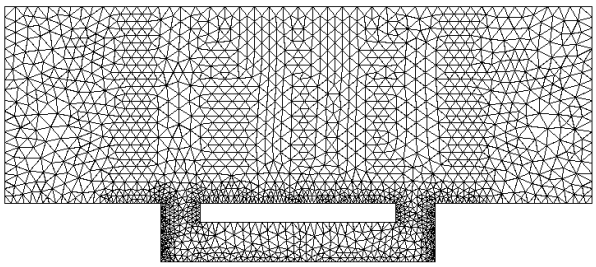

Figure 11 A typical computational grid

A typical computational grid is shown in Figure 11. At the inlet boundary, the stagnation pressure profile was chosen so as to create a linear velocity profile. A linear velocity profile is used because only the very near wall region (i.e. in the laminar sublayer) of the boundary layer is modelled in the computation. The computational domain extends to between 1.25 and 6.25 wall units, depending on the Reynolds number, from the wall. This is equal to a length of the sensor in the streamwise direction. Because only the near wall flow is computed, no turbulence model was employed. The inlet stagnation temperature and the exit static pressure were assumed to be uniform. A full-slip condition was applied to the upper surface of computational domain and the no-slip condition was applied to all of the other surfaces.

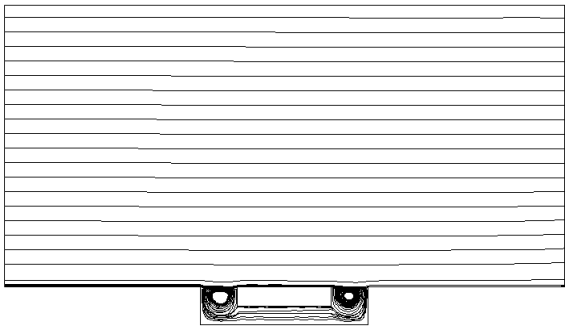

(a) Entire computational domain

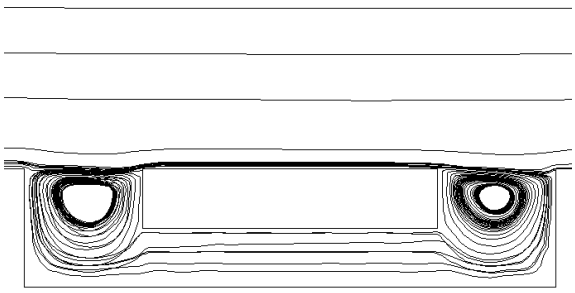

(b) Flow around sensor

Figure 12 CFD calculated flow pattern around the chosen sensor cross section.

The critical wall roughness height is approximately 5 wall units. The purpose of the CFD calculations was to determine if the cavity around the sensor caused any disturbance in the main flow. Several different cross sectional geometries of the sensor bridge and of the cavity were examined using the CFD. Alterations to the wake and height of the cavity, inclined cavity sidewalls, and sensors extending into the main flow were all considered. However, the cross section that consisted of vertical sidewalls with the top surface of the sensor flush with the main surface was found to cause the least disturbance. This is also a simple geometry to manufacture using micromachining techniques. The flow pattern over and around this cross section was also evaluated using a water flume and it was found that it gave results that were very similar to those provided by the CFD calculation.

The results of the CFD computation for the best configuration are shown in Figure 12. The gap beneath the bridge is equal to the depth of the bridge. The streamwise length of the sensor is five times the depth of the bridge. It can be seen that the main flow passes over the sensor and it is undisturbed by the presence of the cavity around the sensor. Within the cavities, there are vortices. The strengths of these vortices are affected by the shape and size of the cavity. In this case, the vortices are extremely weak and there is almost no flow underneath the bridge. The flow underneath the bridge occurs in the upstream direction in this particular case. The very low of velocities are desirable because the convective heat transfer is then reduced to negligible proportions underneath the bridge.

MANUFACTURING

The proposed shear stress sensor has not been manufactured but the outline of the manufacturing procedure is given below. The process starts with n-type (100) silicon wafers. First a layer of polysilicate glass (PSG) of about 2 μm is deposited using the low-pressure chemical vapour deposition (LPCVD) process. This PSG layer is patterned by photolithography and then etched by RIE to form a rectangular shape. The cross-section view is shown in Figure 13. Another PSG layer of about 0.5μm thick is deposited, patterned and etched. The cross-section view after this step is shown in Figure 14. This PSG structure forms the sacrificial part for the bridge and will be removed later to form the space underneath the bridge structure. Note the PSG will be deposited in two steps to round off the corner of the sacrificial layer. The purpose is try to make a smoother connection between the sensor on top of the bridge and the electrical leads and so to reduce regions of concentrated current density in the connections and the sensor.

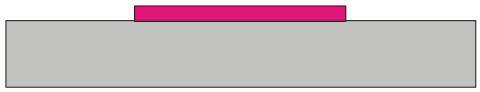

Figure 13 Cross section view after the etching of the first layer of PSG.

Figure 14 Cross section view after the etching of the second layer of PSG

The bridge structure can be made in several ways, depending on the selected sensor material and the desired sensor resistance. It is possible to use polysilicon for the bridge structure and as the electrical conductor. This would be very simple, but the electrical resistance of the sensor will be very high and there would need to be a connection between polysilicon and the external electrical leads. An alternative method was therefore selected.

To manufacture this sensor, a layer of silicon nitride with a thickness of about 0.5 μm is deposited, patterned and etched by RIE to form the bridge structure as shown in Figure 15.

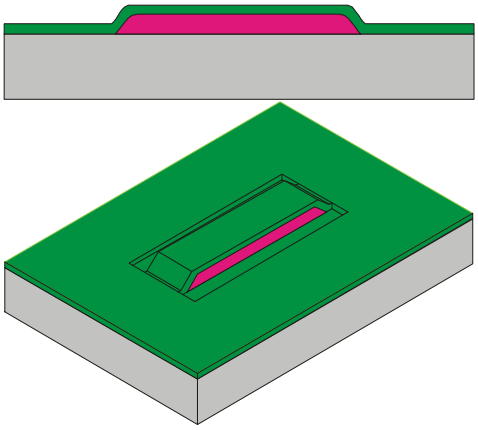

Figure 15 Form the bridge structure by silicon nitride.

The thin-film is created by sputtering a 0.1 μm layer of silver (shown in red). The unwanted silver is removed by a technique called "lift-off" (Madou). A further 0.2μm thick silver is deposited and structured to increase the conductivity of the leads, which ensures that the potential difference across the active part of the sensor is significantly greater than that across the leads. The structure after this step is shown in Figure 16. The width of the bridge is about 5μm. The sacrificial PSG layer is removed at this time by hydrofluoric acid (HF).

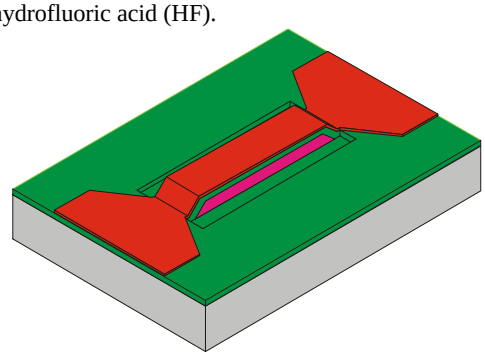

Figure 16 The bridge structure after the deposition of metal connection and before the removal of the sacrificial layer

The final step is to create a surface that is flat and flush with the top of the sensor. A PSG layer with a thickness equal to the height of the bridge (3μm) is deposited by LPCVD. The part of PSG layer on top of the bridge structure with a length of 106μm and a width of 11μm will be removed by RIE. The final structure is a freestanding bridge with a 3μm gap all around as shown in Figure 17.

If it is required, a final mask can be used to pattern a rectangle to form a cavity on the underside of the silicon wafer by backside etching. The size of the rectangle should be such that it leads a membrane that is 50 μm longer and wider than the size of the cavity and around the sensor.

CONCLUSIONS

A new design of wall shear stress sensor, based on the principles of thermal anemometry, has been proposed. The design has an improved frequency response and a much reduced thermal footprint when compared to conventional sensors. These improvements are achieved by reducing the size of the sensing element in order to decrease the thermal mass of the system and by thermally isolating the sensor from the substrate. The thermal isolation is achieved by mounting the thin-film on a suspended bridge. CFD calculation and flow visualisation experiments showed that because the cavity around the sensor is very small, the shear stress sensor is not expected to cause any disturbance to the main flow.

It was also argued that the proposed design, because it eliminates the thermal footprint, should have an improved yaw sensitivity. Furthermore, the proposed sensor had a much improved sensitivity to wall shear stress as less heat is conducted into the substrate as a result of the physical separation of the heated element from the substrate.

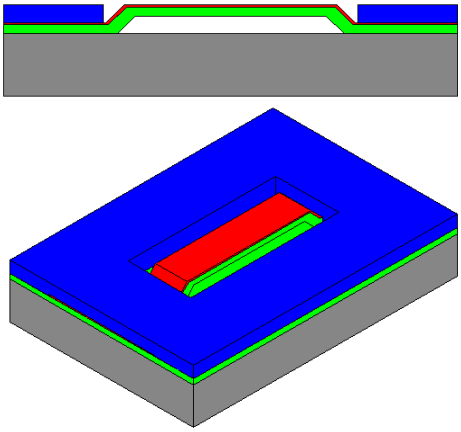

Figure 17 The completed sensor

REFERENCES

B.J. Bellhouse, D.L. Schultz, 1966, "Determination of mean and dynamic skin friction, separation and transition in low-speed flow with a thin-film heated element", Journal of Fluid Mechanics, vol 24, pp. 379-400

Dawes, W N, 1993, "Simulating unsteady turbomachinery flows on unstructured meshes which adapt both in time and space" ASME Paper 93-GT-104, Cincinnati, May

Freymuth, P, 1977, "Frequency Response and Electronic Testing for Constant-Temperature Hot-Wire Anemometers", J Phys E, vol 10, pp705-710

Goldstein, RJ, 1983, Fluid Mechanics Measurements, Hemisphere Publishing Corporation, London

Liu, C, Huang, J-B , Zhu, Z, Jiang, F, Tung, S, Tai, Y-C, and Ho, C-M, "A Micromachined Flow Shear-Strett Sensor Based on Thermal Transfer Principles", Journal of Microelectromechanical Systems, vol. 8, pp. 90-98, March 1999

Madou, M, 1997, "Fundamentals of Microfabrication", CRC Press, New York